Supplement of Atmos. Chem. Phys., 26, 9493–9508, 2026
https://doi.org/10.5194/acp-26-9493-2026-supplement

Atmospheric Chemistry and Physics
Open Access
EGU

Supplement of

The changing sensitivity of wintertime particulate nitrate to precursor emissions diagnosed via GEOS-Chem and satellite observations of ammonia and nitrogen dioxide over the Midwestern United States

Toan Vo and Amy E. Christiansen

Correspondence to: Amy E. Christiansen (achristiansen@umkc.edu)

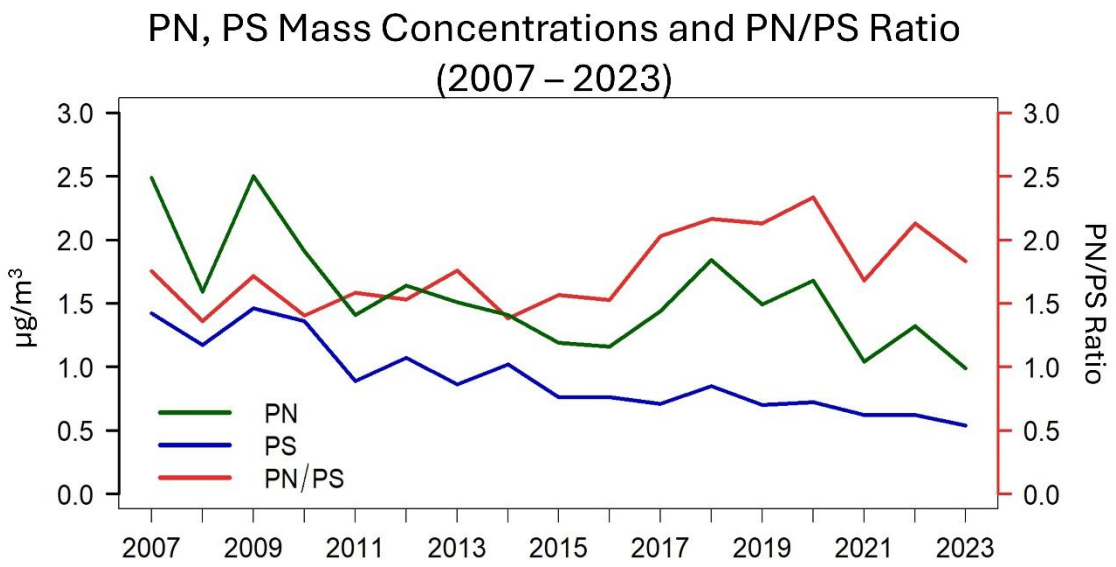

Figure S1: Wintertime PN mass concentrations (green), PS mass concentrations (blue), and PN/PS ratios (in red) over the MWUS from 2007 to 2023.

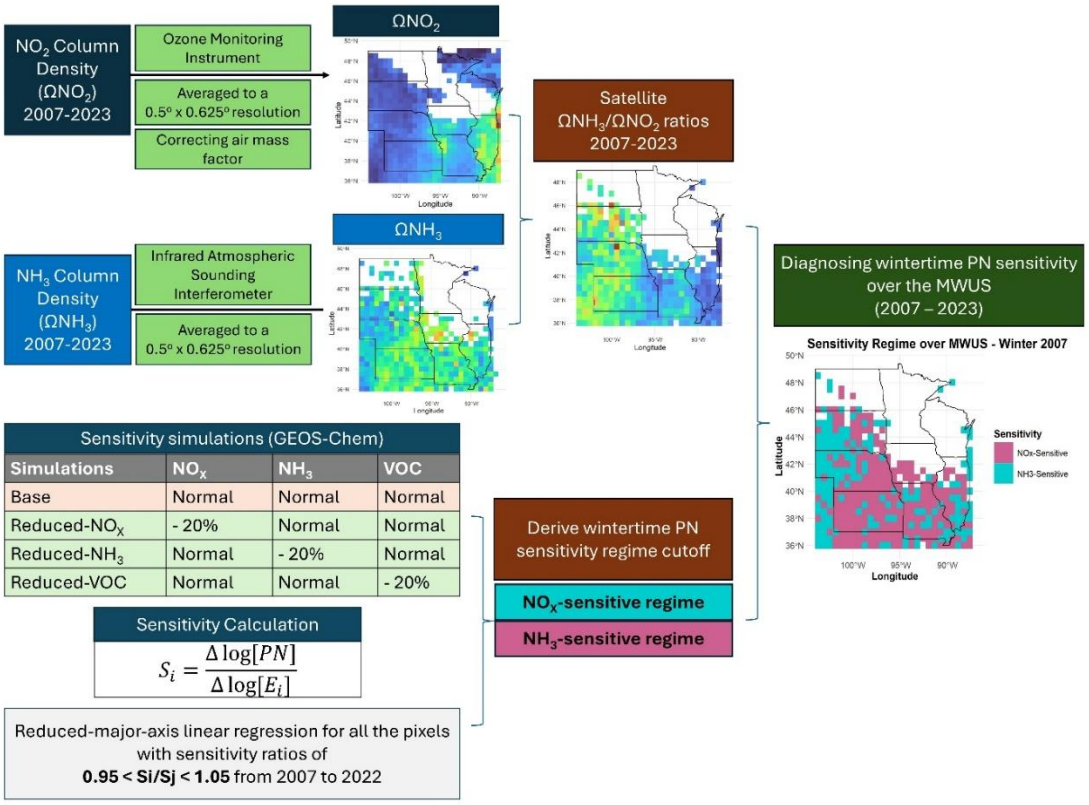

Figure S2: Overview of the methodology of this project. For the satellite analysis, we first retrieved information for NO_2 and NH_3 column densities from the Ozone Monitoring Instrument (OMI) and the Infrared Atmospheric Sounding Interferometer (IASI) from 2007 to 2023. After applying the filtering conditions for the data, we spatially averaged both NO_2 and NH_3 column densities to a 0.5° x 0.625° resolution to match with GEOS-Chem resolution. Air mass factor corrections were applied to OMI NO_2. We then

overlaid the 0.5° x 0.625° composites of NH_3 and NO_2 column density to compute the satellite NH_3/NO_2 ratios. Next, we performed several sensitivity simulations via GEOS-Chem, the descriptions of which are discussed in section 2.2, from winter 2007 to winter 2022. Using solely GEOS-Chem outputs, we calculated the sensitivity of wintertime PN to each precursor gas. These sensitivities were then used to derive formation regime cutoffs by performing reduced-major-axis linear regression. Lastly, we applied these model-derived cutoff equations to the satellite-derived NH_3/NO_2 ratios to diagnose the formation sensitivity of wintertime PN to precursor gases.

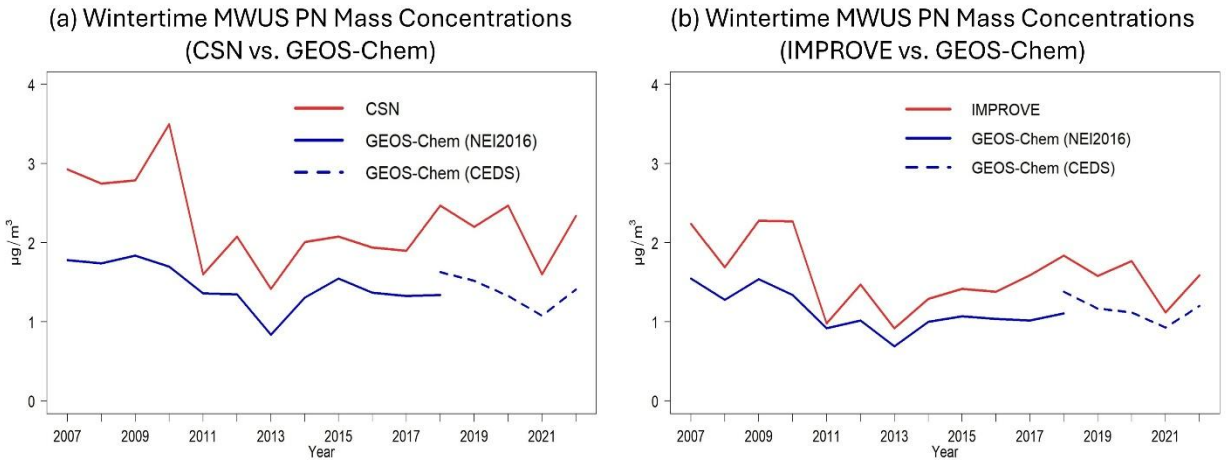

Figure S3: The comparisons in wintertime PN trends between ground monitoring observations, (a) CSN and (b) IMPROVE, and the Base simulation in GEOS-Chem. Solid red lines represent the wintertime PN mass concentrations from ground monitoring observations (IMPROVE and CSN). Solid blue lines represent the wintertime PN mass concentrations from GEOS-Chem using NEI2016 emissions inventory. Dashed blue lines represent the wintertime PN mass concentrations from GEOS-Chem using CEDS emissions inventory.

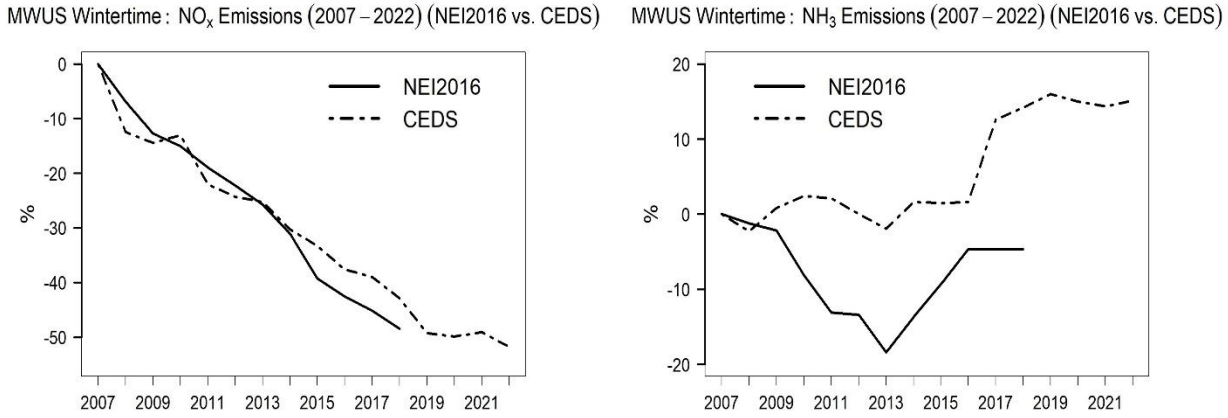

Figure S4: The percentage changes relative to 2007 of wintertime NO_x emissions (left) and NH_3 emissions (right) using NEI2016 (solid lines) and CEDS emissions inventories (dashed lines and points) over the MWUS (2007–2022).

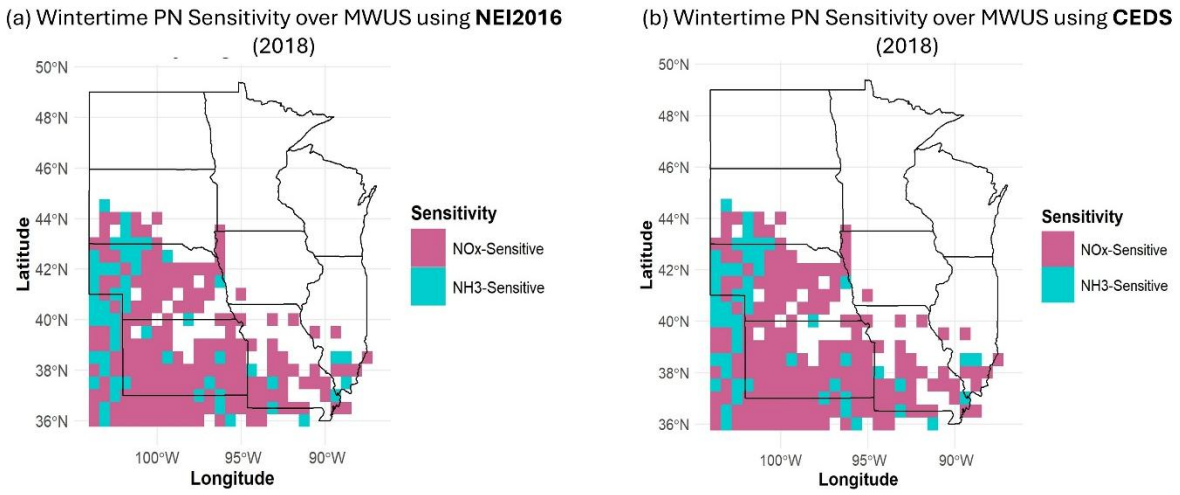

Figure S5: Wintertime PN sensitivity in winter 2018 (i.e., Jan 2019) using NEI2016 emissions inventory (left) and CEDS emissions inventory (right). Pink pixels indicate PN formation is sensitive to NO_X emissions (i.e., NOx-sensitive), and blue pixels indicate PN formation is sensitive to NH_3 emissions (i.e., NH_3-sensitive).

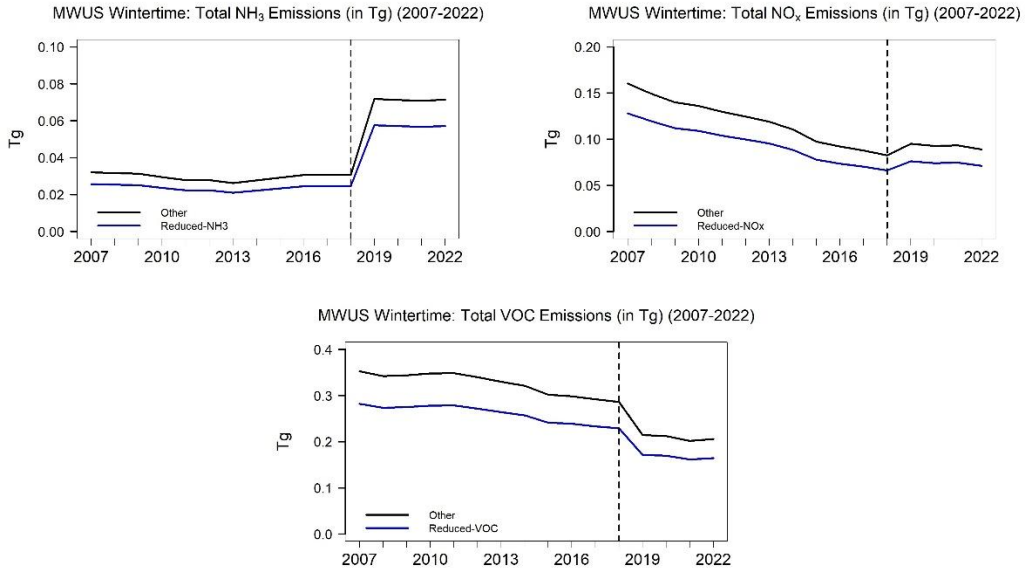

Figure S6: Total NO_x, NH_3, and VOC emissions in Tg from 2007 to 2022 over the MWUS. Panel (a) shows the total NO_X emissions for the Reduced-NH_3 simulations and all other simulations ("Base", "Reduced-NO_x", and "Reduced-VOC simulations). Panel (b) shows the total NO_x emissions for the Reduced-NO_x simulations and all other simulations ("Base", "Reduced-NH_3", and "Reduced-VOC" simulations). Panel (c) shows the total VOC emissions for the Reduced-VOC and all other simulations ("Base", "Reduced-NH_3", and "Reduced-NO_x" simulations). The vertical dashed line at 2018 represents the switching of emissions inventories from NEI2016 to CEDS due to limited availability of NEI2016.

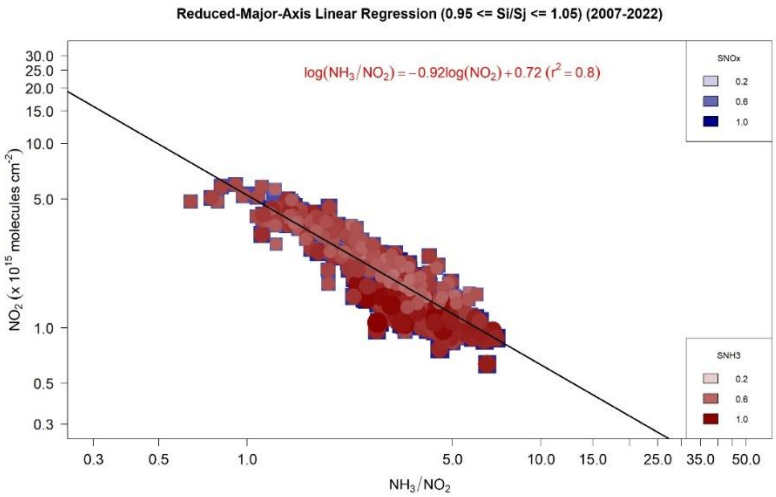

Figure S7: Wintertime PN regime cutoffs derived using reduced-major-axis linear regression for the whole timeframe. The data points shown represent independent model grid cells that show no dominant regime ($0.95 \leq S_i/S_j \leq 1.05$). The colors of the data points are the GEOS-Chem-calculated sensitivity (S_i) in those grid cells. The regression equation is shown at the top.

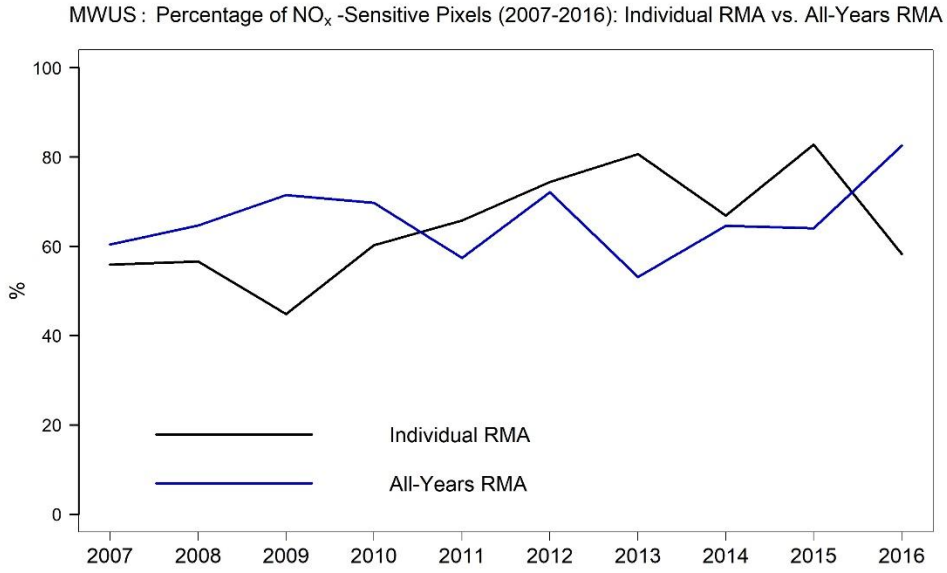

Figure S8: The comparison of the percentage of NO_x-sensitive pixel counts over the MWUS as a result of using individual-year regression (in black) and all-years regression (in blue).

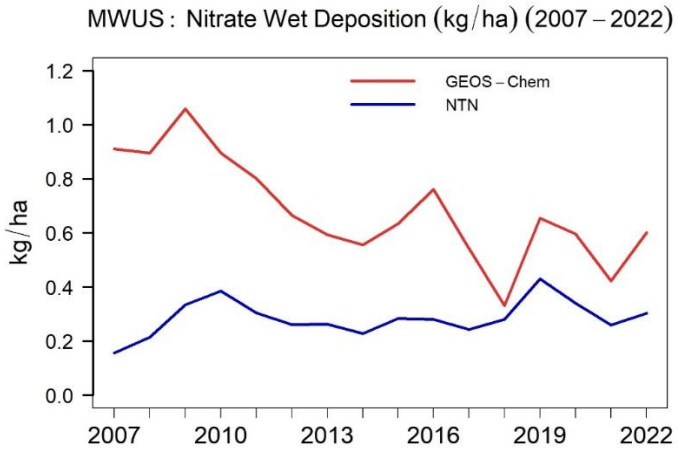

Figure S9: Comparison of wintertime nitrate wet deposition over the MWUS between GEOS-Chem and National Trends Network. Blue line represents of nitrate wet deposition from the ground monitoring network. Red line represents nitrate wet deposition from GEOS-Chem.

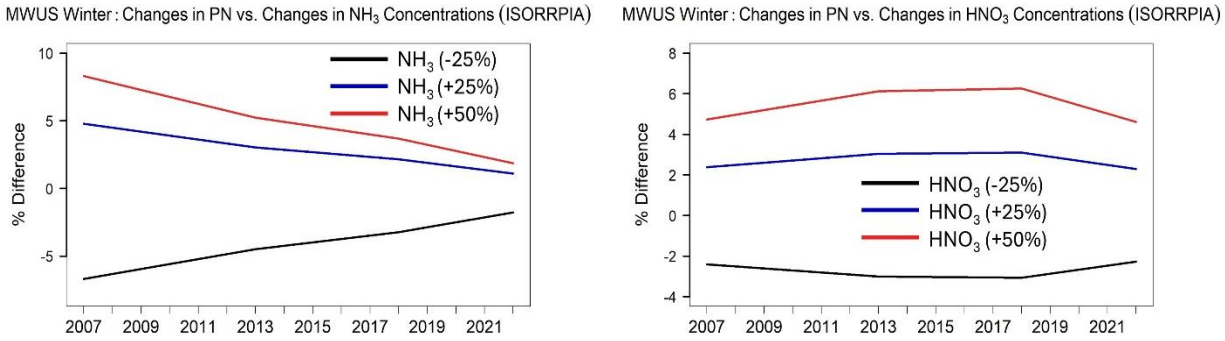

Figure S10: The changes in thermodynamic regime of wintertime PN formation at surface level using ISORROPIA-II. Panel (a) shows the percent changes in PN in response to changes in NH_3 concentrations by -25% (in black), +25% (in blue), and + 50% (in red). Panel (b) shows the percent changes in PN in response to changes in HNO_3 concentrations by -25% (in black), +25% (in blue), and + 50% (in red).

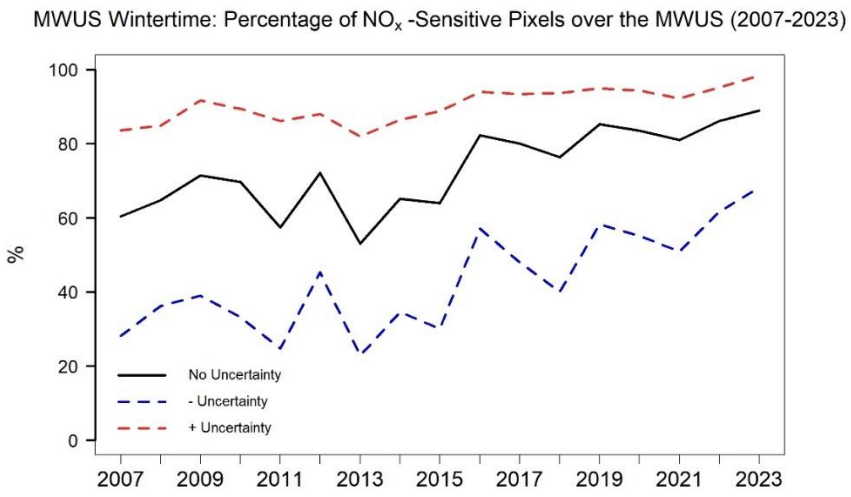

Figure S11: The uncertainty of diagnosed NO_x-sensitive grid cells in classifying wintertime PN formation regime. The solid black line represents the percentage of NO_x-sensitive pixel counts using the standard satellite NO_2 and NH_3 column densities (i.e., no uncertainties applied). The dashed blue line represents the percentage of NO_x-sensitive pixel counts using the low-extreme end of the uncertainty ranges of satellite observations. The dashed red line represents the percentage of NO_x-sensitive pixel counts using the high-extreme end of the uncertainty ranges of satellite observations.

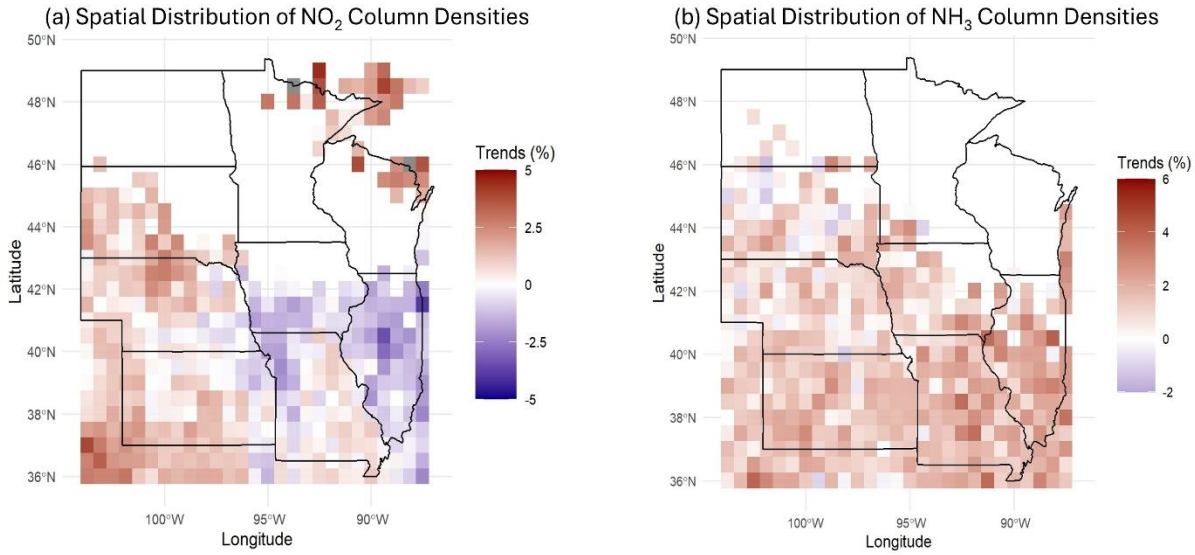

Figure S12: The average percent change in wintertime (a) NO_2 and (b) NH_3 column density over the MWUS (2007–2023). Increases are shown in red, and decreases are shown in blue. Grey pixels indicate an increase > 5% in NO_2 column density for panel (a) only.

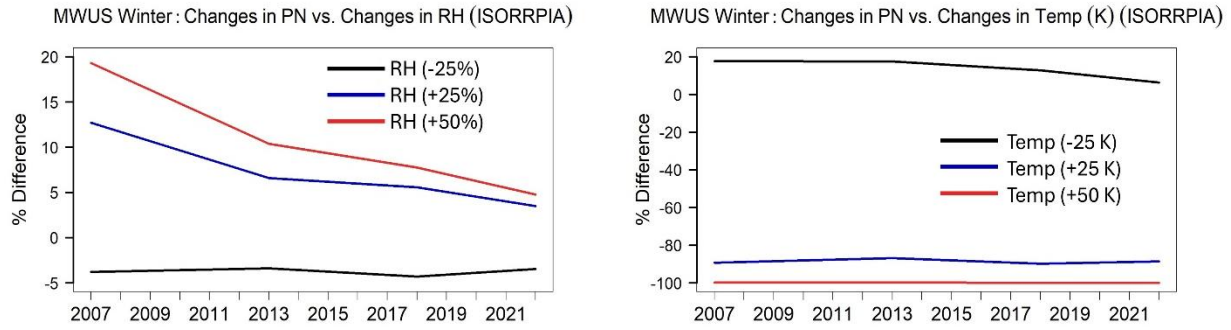

Figure S13: The changes of wintertime PN in response to changes in (a) relative humidity and (b) temperature (in K) at surface level using ISORROPIA. The black lines represent the changes in PN when RH is decreased by 25% in panel (a), and temperature is decreased by 25 K in panel (b). The blue lines represent the changes in PN when RH is increased by 25% in panel (a), and temperature is increased by 25 K in panel (b). The red lines represent the changes in PN when RH is increased by 50% in panel (a), and temperature is increased by 50 K in panel (b).

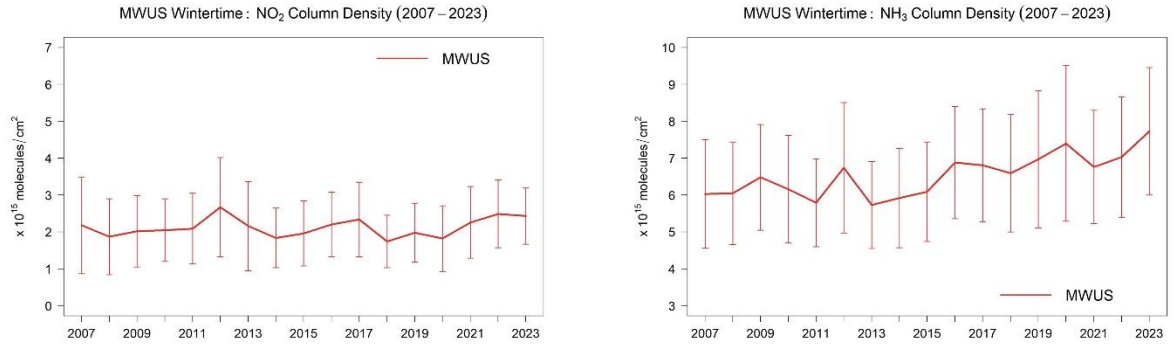

Figure S14: The trends of satellite (a) NO_2 column densities and (b) NH_3 column densities with error bars. The error bars represent ± 1 standard deviation.

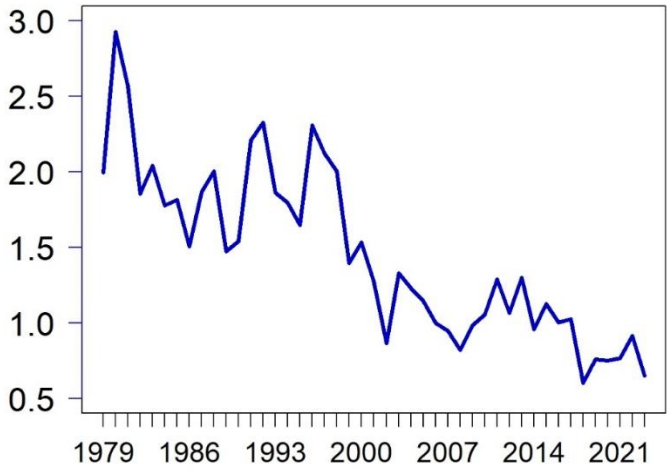

Figure S15: Wintertime nitrate wet deposition (NWD) trends over the MWUS from 1979 to 2023 using the National Trends Network.

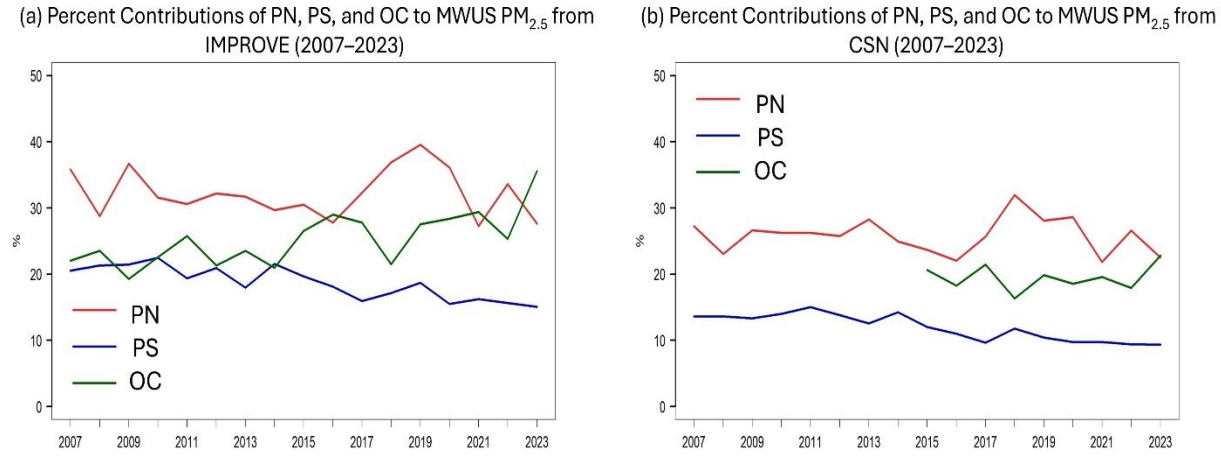

Figure S16: The contributions of PN (red), PS (blue), and total organic carbon (OC) (green) to total $PM_{2.5}$ trends over the MWUS (2007 – 2023) using (a) IMPROVE and (b) CSN ground monitoring observations.

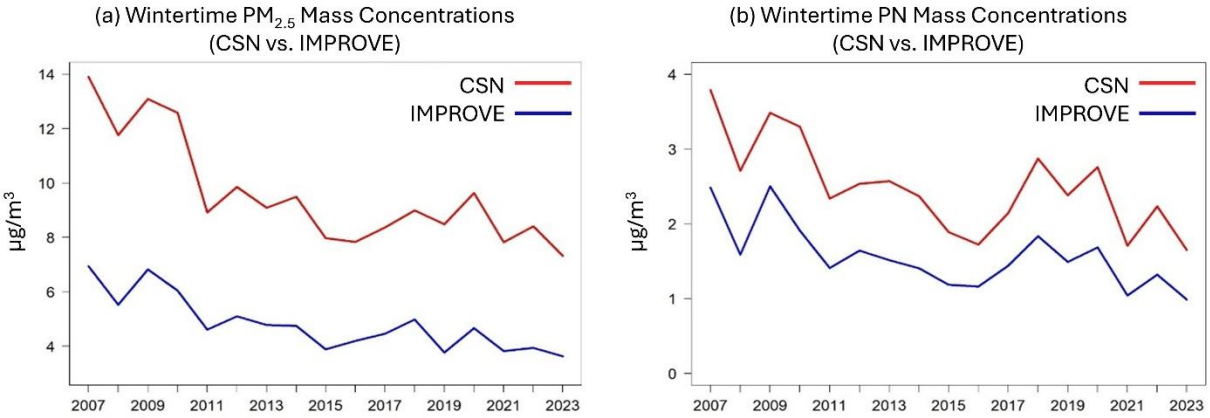

Figure S17: Wintertime $PM_{2.5}$ and PN trends over urban and rural areas in MWUS (2007 – 2023) using IMPROVE (blue) and CSN (red) ground monitoring observations.

S1: The influences of aerosol liquid water (ALW), N_2O_5 uptake, and aerosol residual layers on PN trends.

We first investigate the impact of ALW on wintertime PN formation using the aerosol thermodynamic equilibrium model ISORROPIA-II. Trends in ALW and PN are closely linked (Figure S18), in which both species show a leveling-off of trends after 2010. We suspect this is likely due to the impact PN has on ALW due to its highly hygroscopic nature. We then performed sensitivity simulations with ISORROPIA-II to assess the impact of NH_3 and HNO_3 changes on ALW. We changed NH_3 and HNO_3 gaseous concentrations individually by -25%, +25%, and +50% (Figure S19). Changing HNO_3 concentrations has an increasingly strong impact on ALW over time, suggesting that PN is partially responsible for driving ALW trends. However, changing NH_3 concentrations has a weakening effect on ALW over time. Thus, it is most likely that changes in ALW are not being driven by NH_3 in recent years; rather, they are more strongly influenced by changes in HNO_3.

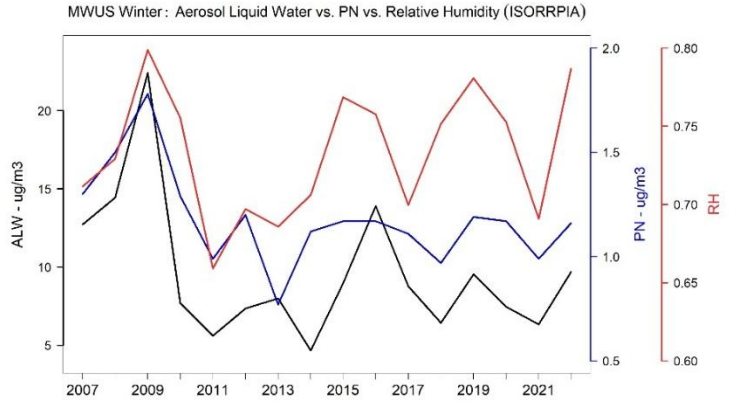

Figure S18: The trends of aerosol liquid water (ALW, in blue), particulate nitrate (PN, in blue), and relative humidity (RH, in red) over the MWUS during wintertime (2007 – 2022).

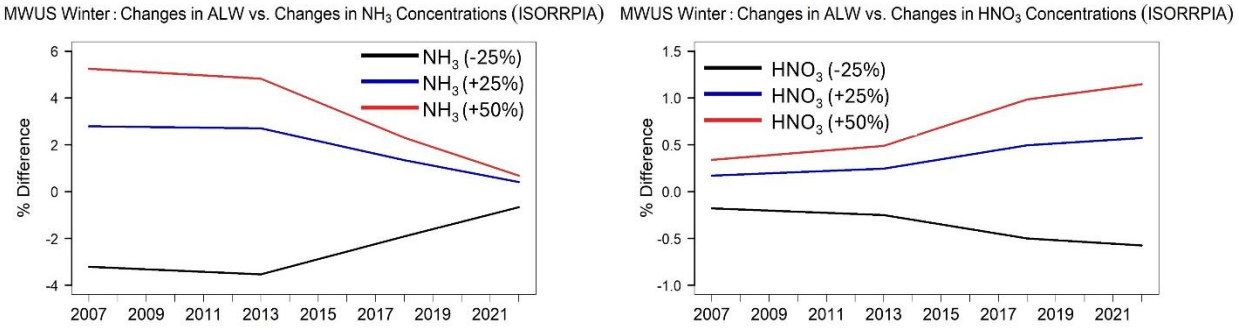

Figure S19: The changes in aerosol liquid water (ALW) in response to changes in (a) NH_3 concentrations and (b) HNO_3 concentrations using ISORROPIA-II. Panel (a) shows the changes in ALW in response to changes in NH_3 concentrations by -25% (in black), +25% (in blue), and + 50% (in red). Panel (b) shows the changes in ALW in response to changes in HNO_3 concentrations by -25% (in black), +25% (in blue), and + 50% (in red).

Next, we address N_2O_5 uptake. Unfortunately, we are unable to quantify trends in N_2O_5 uptake, as the GEOS-Chem diagnostic for uptake coefficients has been non-operational since version 13.3.0. Previous studies have indicated that increases in N_2O_5 concentrations may cause an increase in PN formation during winter (Lin et al., 2025). We investigated trends in N_2O_5 concentrations from GEOS-Chem and found that N_2O_5 concentrations have decreased slightly over time as shown in Figure S20 (-0.0027 ± 0.0004 ppb yr^{-1}). While changes in N_2O_5 uptake may be a possible driver of PN trends that adds uncertainty to our analysis, the small trends in N_2O_5 concentrations suggest that uptake of N_2O_5 is unlikely to play a major role.

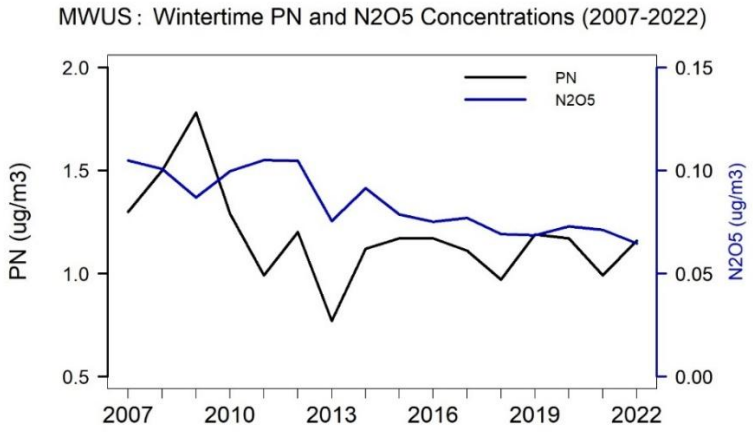

Figure S20: The trends of wintertime PN and N_2O_5 concentrations over the MWUS (2007 – 2022).

There is also evidence in the literature of PN concentrations being impacted by the residual aerosol layers in the upper planetary boundary layer, which also adds uncertainty to the trends in PN (Curci et al., 2015). However, Tang et al. (2021) found that PN in the residual layer is much lower than surface-level PN due to lower RH, which suppresses PN formation (Tang et al., 2021). Thus, we assume that wintertime PN will not be largely impacted by residual layer PN, as RH is low during winter.

S2: Diagnosing wintertime PN formation sensitivity and the influence of meteorology using thermodynamic model (ISORROPIA-II)

We performed several sensitivity simulations to diagnose wintertime PN formation sensitivity using ISORROPIA-II, which was used to calculate thermodynamic partitioning between gaseous HNO_3 and particle phase PN (Fountoukis and Nene, 2007). We chose to perform the simulations at various time slices (2007, 2013, 2018, and 2022) to observe the responses of PN to meteorological parameters and thermodynamic partitioning processes over time. In all simulations, we ran ISORROPIA-II in forward mode to examine changes in aerosol PN. The inputs were from GEOS-Chem, including temperature (in K), relative humidity, and total concentrations (i.e., gas + aerosol) (in $\mu g\ m^{-3}$) of NH_3, HNO_3, and H_2SO_4.

We first conducted several sensitivity simulations to study the impacts of meteorology on the formation of winter PN. We changed temperature by -25 K, + 25 K, and +50 K and changed RH by -25%, +25%, and +50%. We found that the same changes in temperature across our timeframe result in increasingly smaller changes in PN over time. In 2007, decreasing temperature by -25 K results in an 18% increase in PN, while in 2022, the same decrease in temperature results in only a 6% increase in PN (Figure S13). The same is true for RH. In 2007, a 50% increase in RH results in a 19% increase in PN, but it only results in a 5% increase in PN in 2022 (Figure S13). These results suggest that the changes in chemistry are the major driver of changes in wintertime PN rather than meteorological variability.

For thermodynamic partitioning, we changed NH_3 and HNO_3 gaseous concentrations individually by -25%, +25%, and +50%. We found that decreasing NH_3 concentrations produces smaller changes in PN over time: a 25% decrease in NH_3 decreases PN by -7% in 2007, but only -2% in 2022. Ramping up NH_3 concentrations also showed similar patterns: a 50% NH_3 increase in 2007 results in an 8% increase in PN, while that same increase in 2022 only results in a 2% increase in PN (Figure S10). These results suggest that PN is becoming less sensitive to NH_3. By contrast, the influence of HNO_3 on PN remains consistent over time. Decreasing HNO_3 concentrations by 25% leads to a steady -2% decrease in PN from 2007 to 2022. Similarly, ramping up HNO_3 concentrations significantly increases the production of PN consistently over time (~5%). These results suggest that MWUS PN is becoming thermodynamically less NH_3-sensitive and more HNO_3-sensitive, but on average may not be fully moved into HNO_3-sensitivity (i.e., in transition). Our ISORROPIA-II results suggest that the aerosol thermodynamics are consistent with our satellite-based diagnosis, in which we find that many areas of the MWUS have shifted away from NH_3-sensitivity.